Trans Indian Inst Met
https://doi.org/10.1007/s12666-024-03364-2

ORIGINAL ARTICLE

A Prediction Model Based on Simulation (FEA) and Response Surface Methodology (RSM) for Sintered Al–TiB_2 Preforms

Md. Ahasan[1] · D. S. Chandramouli[1,2] · Ratnala Prasad[1] · Nalla Pradeep[3] · Ch. Shashikanth[4]

Received: 21 February 2024 / Accepted: 20 May 2024

Abstract The current study centers on two techniques: neural network (NN) and response surface methodology (RSM), applied to predict the final density (FD) of sintered aluminum preforms. In this work, the load, the aspect ratio and the initial preform density were taken as input parameters and the response (output) variable measured was FD. Prediction for the response variable FD was obtained with the help of empirical relation between the response and the input variables using RSM's (RSM) Box–Behnken design of experimental technique and also through Neural Network (NN). Predicted values of the response by both the techniques, i.e., RSM and NN were compared with the experimental values and their closeness with the experimental values was determined. Moreover, it has been discovered that the aspect ratio has minimal impact on densification and that the FD of the preform rises with both the load applied and the initial preform density of the sintered preforms. The authors were able to predict the FD of sintered preforms of Al–TiB_2 for different initial preform and aspect ratio conditions by using NN and RSM techniques.

Keywords Neural network (NN) · Response surface methodology (RSM) · Sintered aluminum · Powder preforms · Cold axial forming

Abbreviations

Adeq precision	Adequate precision
Adj. R^2	Adjusted R^2
DF	Degrees of freedom
FD	Final density
Pred. R^2	Predicted R^2
R^2	Coefficient of determination
S.D.	Square root of the residual mean square
Cor. total	Totals of all data adjusted for mean
C.V.	Coefficient of variation
Prob. > F	Percentage of the probability or time you would expect to obtain the specified F value
A	First variable or factor examined—load (LD)
B	Second factor or input variable investigated—aspect ratio (ASPR)
C	Third factor or input variable investigated—initial preform density (IPD)
PRESS	Expected sum of squares for residual error

1 Introduction

Understanding the densification behavior of sintered aluminum preforms during forming is very important in

✉ D. S. Chandramouli
dkmouli1986@gmail.com

Md. Ahasan
mdahasankhan@gmail.com

[1] Department of Mechanical Engineering, Aditya College of Engineering & Technology (A), Surampalem, AP 533437, India

[2] Department of Mechanical Engineering, MallaReddy Engineering College (A), Hyderabad, Telangana 500100, India

[3] Department of Mechanical Engineering, Sasi Institute of Technology & Engineering, W.G, Tadepalligudem, A.P 534101, India

[4] Department of Mechanical Engineering, Sree Chaitanya College of Engineeing, Karimnagar, Telangana 505527, India

Published online: 25 July 2024

achieving quality powder metallurgy (P/M) parts. For P/M materials, there is a well-established dependence of strength upon density [1]. The densification behavior of the P/M (Powder Metallurgy) product deviates significantly from conventional cast and wrought materials due to the presence of air gaps in the aluminum preforms. For instance, compared to typical materials, porous materials spread less in the transverse direction when squeezed. Additionally, during deformation, densification and cold working of the base metal both generate an increase in flow stress [2, 3]. However, the sintered preforms can be deformed again to a final size within reasonable dimensional tolerance to increase its density very close to fully dense materials [2]. Kuhn et al. [3] has reported that by using cylindrical specimens in uniaxial compression experiments, the basic mechanical reactions of porous metals—densification, plastic flow, and fracture—can be determined. A portion of the metal flows into the pores during the compressive deformation of the sintered powder metal preform, causing the bulk volume to decrease. As the metal fills the pores, simultaneously the preforms density increases [4]. Comprehending the distribution of the density during the compaction and understanding the behavior deformation of powder preforms throughout forming are crucial for producing high-quality Powder Metallurgy (P/M) parts. Uneven density distribution can lead to distortion in the final parts [2]. Abdul Rahman et al. [5] has looked into how the preform's relative density affects the forming limit. Mamalis et al. [6, 7] has used the yield criterion to study the porosity and micro-flaws on materials that have undergone plastic deformation. In order to meet end-user demands, P/M component manufacturers are interested in forecasting the ultimate density of their products. It is exceedingly challenging to estimate the ultimate density before experimenting, though. In the industrial sector, modeling approaches are now being employed for process parameter prediction and optimization. Neural networks have been used to examine the deformation properties of sintered aluminum preforms. [8, 9]. Response surface technique has been used to evaluate the bead quality of submerged arc pipe welding [10]. However, not much work has been done to model the densification behavior of powders under compressive forces. Chandrasekar et al. [14] conducted a study on the dynamic effects of cold upsetting of sintered aluminum truncated conical preforms. The researchers employed DEFORM 3D software to simulate the process and utilized statistical techniques, including response surface method and design of experiments, to forecast and enhance the response. Md. Ahasan et al. [15] DEFORM 2D software, based on finite element analysis (FEA), has been utilized to forecast the distribution of density as well as determine the precise locations of maximum and minimum density zones. Through this analysis, the underlying damage mechanism responsible for the densification process has been identified, and the critical damage value has been successfully determined. Rao et al. [16] predicted values through TLBO and GRA approaches for wear characteristics of composites were notably influenced by changes in the WC volume percentage (5–25%). Enhanced wear tracks

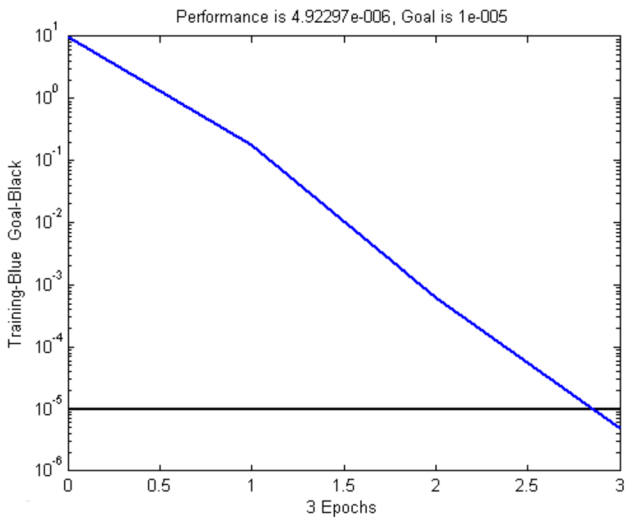

Fig. 2 The correlation between the error value and the epoch count

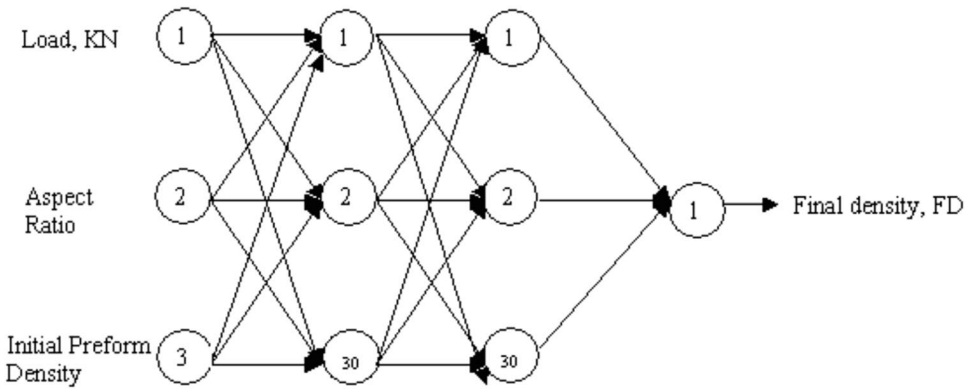

Fig. 1 NN topology with four layers of backpropagation

and closely positioned grooves were observed on the worn surfaces of the composite pin with a higher volume fraction of WC particles. Gangadhara Rao Ponugoti et al. [17] recorded the tribological property indicators, namely the wear rate and coefficient of friction and used as the basis for developing regression models. These models were then checked for adequacy using ANOVA and subsequently utilized for optimization purposes. To derive the values of the optimal control variables, fuzzy gray relational analysis (FGRA) was employed. The effectiveness of this multi-response optimization approach, which aims to minimize both the wear rate and coefficient of friction simultaneously, was thoroughly analyzed and reported. Finally, the validation experimental results confirmed the derived optimal tribological conditions of the composites. Zhang et al. [18] simulated and predicted the fracture in sintered materials using the FEA method. They analyzed the density distribution, strain distribution, and stress distribution in preforms upset up to 50% height reduction. They were able to determine the formability limits for aluminum 601 AB alloy under various initial preform conditions and aspect ratio.

In this paper, the density attained by sintered Al–TiB_2 preforms when they were subjected to cold axial forming operation has been critically discussed. Axial compression tests were conducted on sintered Al–TiB_2 of aspect ratios 0.50, 0.75, and 1.00 and initial preform density values of 0.85, 0.885, and 0.92. Using the Box–Behnken Design of Experiments (D.O.E) approach of RSM, a mathematical model has been built that incorporates the load, aspect ratio, and initial preforms density. The primary and secondary impacts of the process parameters on the density of the sintered Al–TiB_2 powder metallurgy preforms within the scope of analysis were examined using ANOVA. Also, a four-layered back propagation Neural Network has been used to model the densification behavior of sintered Al–TiB_2. In addition to the developed models, additional experiments have been conducted to verify their accuracy. The NN and RSM techniques were applied to predict the FD of the prefoms; the predicted results were very close to the experimental values and to find the behavior of sintered preforms.

2 Experimental Work

This experiment utilized high-purity atomized aluminum powder. The powder was used to form compacts with several aspect ratios or height-to-diameter ratios; these first ratios were 0.50, 0.75, and 1.00. By using various compacting pressures on the aluminum powder in a universal testing machine, compacts with these initial aspect ratios were created, yielding initial compaction densities of 85%, 88.5%, and 92% of the theoretical density. Molybdenum disulphide (MoS_2) served as a lubricant for the die, punch, and butt during compact preparation. The sintered Al–TiB_2 preforms were then compressed according to the design matrix developed by RSM Box–Behnken method. The FD achieved during each stage of applied load was measured using Archimedes principle. For the design, implementation, and simulation of the neural network with feedforward backpropagation algorithm, the MATLAB NN toolbox was employed.

Table 1 Input parameters and their levels

S. no	Parameter	Low level	High level
1	Load (LD)	20	60
2	Aspect ratio (ASPR)	0.50	1.00
3	Initial preform density (IPD)	0.85	0.92

Table 2 Experimental layout for the Box–Behnken design

Std no	Run no	Factor			FD
		LD	ASPR	IPD	
1	7	20	0.50	0.8850	2.4820
2	4	60	0.50	0.8850	2.5969
3	10	20	1.00	0.8850	2.4924
4	1	60	1.00	0.8850	2.5945
5	16	20	0.75	0.8500	2.3694
6	3	60	0.75	0.8500	2.5569
7	17	20	0.75	0.9200	2.5283
8	9	60	0.75	0.9200	2.6168
9	6	40	0.50	0.8500	2.4962
10	13	40	1.00	0.8500	2.4612
11	8	40	0.50	0.9200	2.5794
12	5	40	1.00	0.9200	2.5670
13	2	40	0.75	0.8850	2.5210
14	11	40	0.75	0.8850	2.5210
15	12	40	0.75	0.8850	2.5210
16	15	40	0.75	0.8850	2.5210
17	14	40	0.75	0.8850	2.5210

3 NN Training and Validation

The densification behavior of sintered aluminum preforms has been modeled using a three-layered back propagation NN, as detailed in Ref. [9]. Back propagation NN consists of several layers, including linear output layers and hidden layers that use sigmoid transfer functions. Since the transfer function in hidden layers needs to be differentiable, log

Table 3 Model summary statistics

Source	Std. dev	R^2	Adj. R^2	Pred. R^2	PRESS	
Linear	0.019	0.9130	0.8929	0.8203	0.019	
2FI	0.015	0.9596	0.9353	0.8021	0.011	Suggested
Quadratic	0.012	0.9835	0.9622	0.7356	0.015	

Table 4 Response surface model (response: FD (FD)) ANOVA table

Source	Sum of squares	DF	Mean square	F value	Prob > F	
Model	0.054000	06	0.008997	039.56	< 0.0001	Significant
A	*0.030000*	01	0.030000	133.58	< 0.0001	
B	*0.000194*	01	0.000194	000.85	0.3774	
C	*0.021000*	01	0.021000	091.40	< 0.0001	
AB	*0.000041*	01	0.000041	000.18	0.6803	
AC	*0.002450*	01	0.002450	010.77	0.0083	
BC	*0.000127*	01	0.000127	*000.56*	*0.4709*	
Residual	0.002274	10	0.000227			
Cor total	0.056000	16				

Table 5 Regression statistics

Std. dev	0.015	R^2	0.9596
Mean	2.530	Adj. R^2	0.9353
C.V	0.600	Pred. R^2	0.8021
PRESS	0.011	Adeq precision	23.271

sigmoid and tan sigmoid functions are commonly utilized. In this investigation, the output layer is subjected to the 'purelin' transfer function, which is a linear transfer function, while the hidden layers are subjected to the 'tansig', or tan sigmoid transfer function. Based on a layer's net input, both transfer functions determine its output. Each hidden layer and the output layer use artificial neurons that are connected by weights that can be adjusted. The network's training function has been selected as 'trainlm', a network training function that updates weight and bias variables using the Levenberg–Marquardt approach.

3.1 Proposed NN Structure

Throughout the investigation, many arrangements of layers and neurons were tested. In the end, two hidden layers, an output layer, and an input layer made up a four-layered network. Three neurons that indicate the aspect ratio, load, and starting preforms density are installed in the input layer. Thirty neurons comprise each buried layer. One neuron in the output layer represents the response variable, FD (FD). Figure 1 displays the network architecture that has been demonstrated. The neural network that was formed was trained over a number of iterations until the $1e-5$ error objective was satisfied given the number of neurons, initial weights, and starting biases.

3.2 NN Training

The multiple data gathered through the above-explained experimental work have been used for training the NN model. Before training the network, the training data were normalized suitably. The training data are fed into the proposed network and after several iterations the network delivered a converged result in a lesser epoch (Fig. 2). The weight values obtained from training the network are preserved. Weights from the trained network are then incorporated into another network that has a similar architecture. It is important to note that the test data used for evaluation do not overlap with the data utilized in the network being trained.

As shown in Table 6, the network's output represents the predicted values. This shows that the NN model is capable of forecasting FD values.

4 Design of Experiments

Experiment design is a useful analytical technique for investigating the influence of process variables on a specific variable—an unknown function of these process variables. It entails setting up the experiments such that pertinent data can be statistically assessed and trustworthy, objective results may be obtained. Statistical validation of

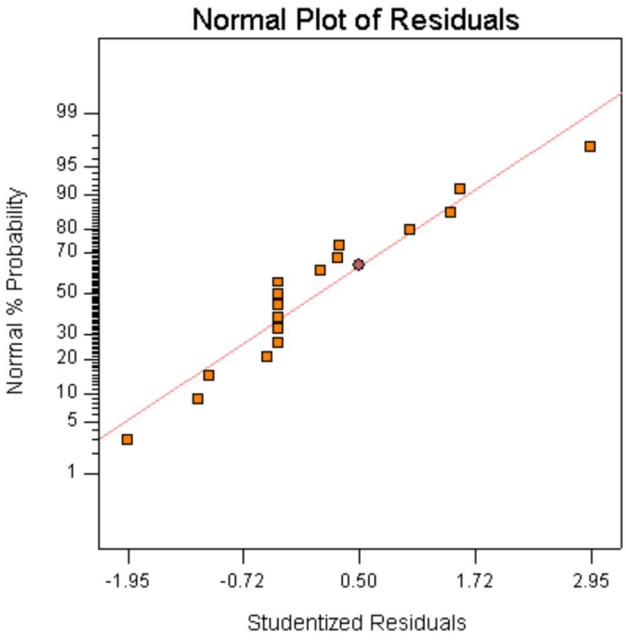

Fig. 3 Plot of residuals with a normal probability for the FD data

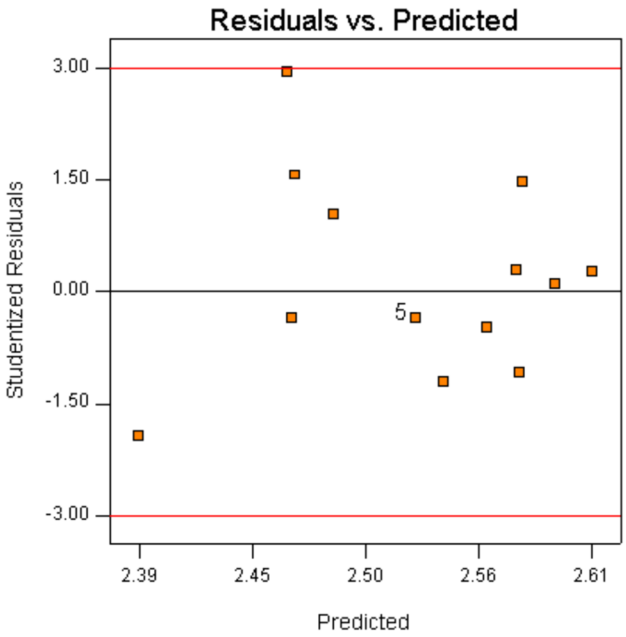

Fig. 4 Plot of the FD's residuals versus the anticipated response

the experimental design is required to extract meaningful insights from the data [11].

5 RSM (RSM)

RSM is a set of mathematical and statistical techniques that are helpful in modeling and assessing engineering issues. The main objective of this methodology is to maximize the response surface, which is a function of several process variables. Furthermore, RSM quantifies the relationship between the generated response surfaces and the input parameters that are under control [11, 12]. The following is the RSM design process [10].

1. Designing a set of tests to capture the relevant answer in a sufficient and reliable approach.
2. Designing a response surface mathematical model with the best fits.
3. Determining the ideal combination of experiment settings to get a response value that is either maximum or lowest.
4. Using two- and three-dimensional charts to illustrate the direct and interaction impacts of the process parameters.

6 Mathematical Model of FD

6.1 Response Equation for FD

Using 17 tests in RSM's Box–Behnken design, the mathematical model for FD was created. The levels that correspond with the input parameters chosen for this challenge are displayed in Table 1. Table 2 provides the FD for each of the 17 assessments. After that, the response equation for the FD is as follows:

$$\begin{aligned} FD = {} & +0.28657 + 0.034852 * (LD) - 0.56556 * (ASPR) \\ & + 2.38643 * (IPD) \quad -0.00064 * (LD) * (ASPR) \\ & - 0.035357 * (LD) * (IPD) + 0.64571 * (ASPR) * (IPD). \end{aligned}$$

7 Confirmation Test

Confirmation experiments were conducted to assess the accuracy of the developed model (Table 6). The confirmation tests' test conditions were selected so that they would fall inside the previously established range of values. The residuals and the percentage error were computed following a comparison of the expected values and the corresponding experimental values. The percentage of errors falls inside allowable bounds. As long as the testing is done within the designated range, the response equation for the FD generated by RSM can therefore be used to precisely predict the FD values for any

Table 6 Partial sample predicted data from the NN and RSM models

Load (LD)	Aspect ratio (ASPR)	Initial preform density (IPD)	FD (FD)		Error %	FD (FD)		Error %
			Experimental	NN predicted		Experimental	RSM predicted	
25	1.00	0.850	2.3801	2.3763	0.15	2.3801	2.4022	0.92
35	0.75	0.850	2.4602	2.4654	0.21	2.4602	2.4536	0.26
45	0.50	0.850	2.5006	2.5010	0.01	2.5006	2.5082	0.30
35	0.50	0.885	2.5308	2.5323	0.05	2.5308	2.5149	0.62
25	1.00	0.920	2.5179	2.5119	0.07	2.5179	2.5526	1.37
45	0.75	0.920	2.5898	2.5878	0.07	2.5898	2.5864	0.13
65	0.50	0.920	2.6294	2.6249	0.17	2.6294	2.6265	0.11

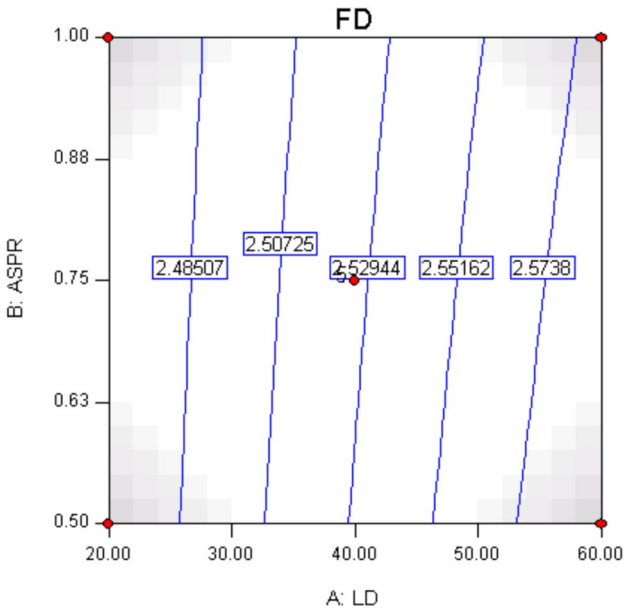

Fig. 5 Contour plot in ASPR-LD plane at IPD = 0.89

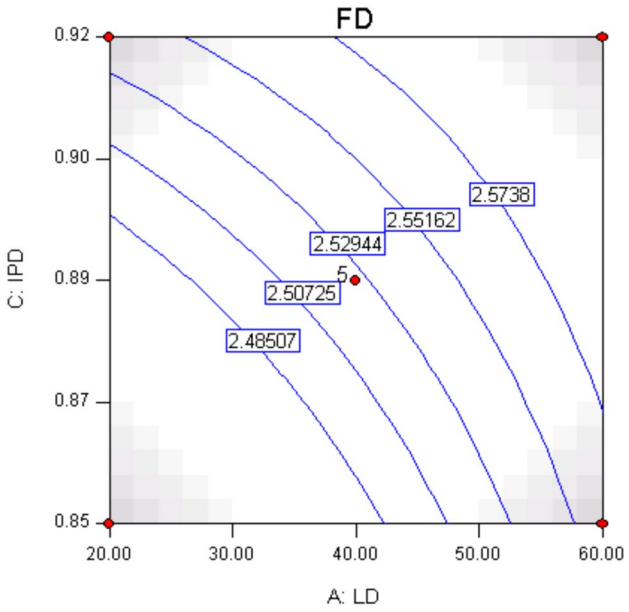

Fig. 6 Contour plot in IPD-LD plane at ASPR = 0.75

combination of the load, the aspect ratio, and the initial preform density values. Additionally, NN can predict density values more accurately than RSM with a tolerable error margin.

8 Results and Discussion

8.1 Response Surface Graphs and ANOVA

Analysis of variance (ANOVA) was used in the study to look at how input parameters affected the FD. According to Table 3's model summary statistics, the 2FI model comes highly recommended. Consequently, this model was used for additional study. The ANOVA for the response surface model with respect to FD is shown in Table 4. One popular method for combining the significance test for each model coefficient is ANOVA. The model's "Prob > *F*" value is less than 0.0500, indicating the importance of the model terms. This is encouraging since it shows that the response is significantly influenced by the terms in the model. The overall relevance of the model is shown by its Model *F* value of 39.56. It is highly unlikely that a significant "Model *F* value" could be the product of random noise, with a chance of only 0.01%.

The regression statistics are shown in Table 5, and the regression model's adequacy is evaluated using the coefficient of determination (R^2). When R^2 is equal to 1, a perfect match is produced; when residuals rise between 1 and 0, R^2 declines. R^2 tends to grow as the number of variables rises since the residuals get smaller. The coefficient of determination adjusted for the degrees of freedom (Adj. R^2) is utilized to improve the accuracy of evaluating the regression model. Adjuvant R^2 compares the range of

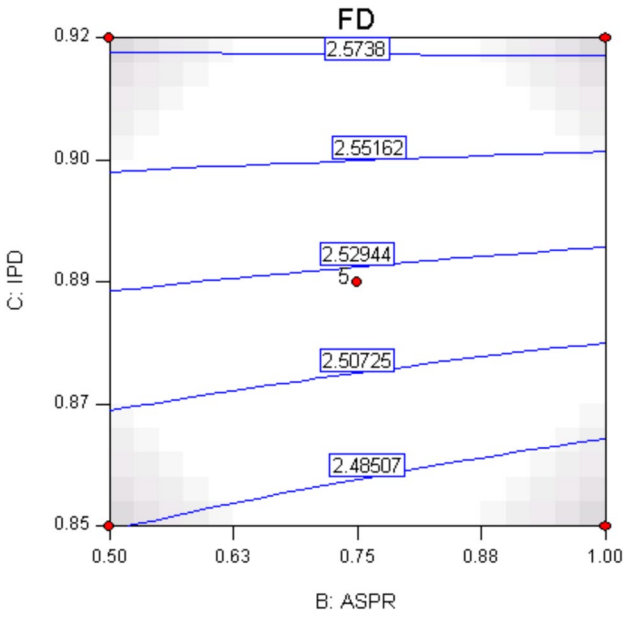

Fig. 7 Contour plot in IPD-ASPR plane at LD = 40

expected values at design points vs. the average prediction error in order to evaluate fit and analyze the residual per unit degree of freedom. A ratio higher than 4 denotes adequate discrimination of the model. The ratio in this instance is 23.271, which is significantly higher than 4, indicating that the model can successfully traverse the response space. Additionally, the Adj. R^2 is 0.9353 and the actual R^2 value is 0.9596. The Adj. R^2 value and the expected R^2 value of 0.8021 are fairly aligned. In this case, the model's efficacy is demonstrated by the high and nearly 1 R^2 value, which is regarded as desirable [13]. The residuals analysis has been utilized to further evaluate the model's suitability [11]. Plots of the residuals vs. predicted response and normal probability plots of the residuals, which show the variations between the projected and observed responses, are used to analyze the remaining data. In a suitable model, the residuals' normal probability plot points should form a straight line. However, the plots of the residuals against the expected response should display an unorganized pattern without any obvious trend [13]. Figures 3 and 4 display the residuals' normal probability plots as well as the plots showing the residuals in relation to the anticipated responses for surface roughness. According to these plots, the residuals often follow a straight line, pointing to a normal distribution of errors. Furthermore, Fig. 4 demonstrates that there is no remarkable structure or trend in the residuals. This finding suggests that the suggested model is sufficient and that neither the independence nor the constant variance assumptions have been broken [13]. Figures 8 and 9 display the 3D surface graphs for the FD. Because the model is sufficient, these 3D surface plots can be used to estimate the FD values for any suitable combination of the input parameters, such as the load, aspect ratio, and beginning preform density value.

A Box–Behnken design was conducted to explore the densification characteristics of sintered aluminum preforms.

Table 6 shows that RSM and NN are both practical methods for estimating the ultimate density of sintered aluminum preforms. When it comes to forecasting the FD with only a few percent error, NN performs better than RSM, according to a comparison study comparing the two algorithms.

In Fig. 5, the contour plot of FD in the ASPR-LD plane at IPD = 0.89 suggests that aspect ratio minimally affects densification. Figure 6, illustrates the contour plot of FD in

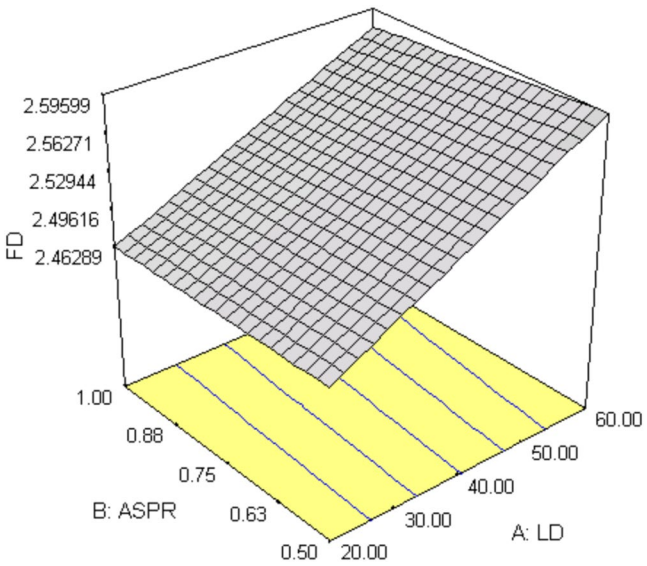

Fig. 8 3D surface graph for the FD (FD) at IPD = 0.89, as ASPR and LD varies

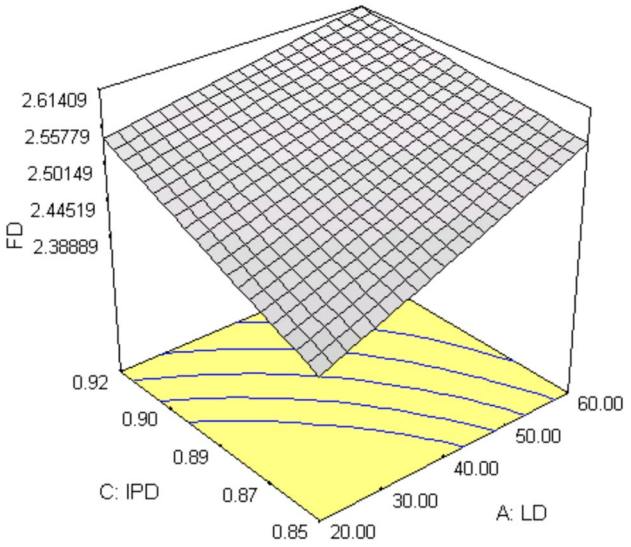

Fig. 9 3D surface graph for the FD (FD) at ASPR = 0.75, as IPD and LD varies

the IPD-LD plane at ASPR = 0.75, indicating that the FD increases with both applied load and initial preform density.

Figure 7, a contour plot of FD in the IPD-ASPR plane at LD = 40, demonstrates that aspect ratio has minimal impact on densification. While aspect ratio has little effect on densification for preforms with lower initial density, it has almost no effect on Preforms with higher initial density.

Lastly, Fig. 8 presents a 3D surface graph for FD at IPD = 0.89, and Fig. 9 displays a 3D surface graph for FD at ASPR = 0.75. These surface plots, validated by the model, can be utilized to navigate and determine the desired FD for various load, aspect ratio, and initial preform density combinations.

Gangadhara Rao Ponugoti et al. [17] investigated tribological property indicators, for the wear rate and coefficient of friction, were recorded and used as the basis for developing regression models. These techniques were then checked for adequacy using ANOVA and subsequently utilized for optimization to predict the values of the optimal control variables. In this paper, authors investigated FD and behavior of Al–TiB_2 preforms by applying NN and RSM models and achieved closer values compared to experimental results.

9 Conclusion

NN and RSM are used in this study to explain sintered Al–TiB_2 preforms density. Using these methods, the ultimate density that sintered Al–TiB_2 preforms achieve is calculated for a range of input factors, including load, aspect ratio, and initial preform density values. It has been found that the load and the initial preform density values are significant parameters, while the aspect ratio is relatively insignificant. Though the design and development of NN is time consuming, it provides accurate results compared with RSM.

Declarations

Conflict of interest The authors declare that they have no conflict of interest.

References

1. Smith L N, Midha P S, and Graham A D, *J Mater Process Technol* **79** (1998) 94.
2. Narayanasamy R, Ponalagusamy R, and Subramanian K R, *J Mater Process Technol* **110** (2001) 182.
3. Kuhn H A, and Downey C L, *Int J Powder Mettal* **7** (1971) 15.
4. Narayanasamy R, and Pandey K S, *J Mater Process Technol* **100** (2000) 87.
5. Abdul-Rahman M, and El-Sheikh M N, *J Mater Process Technol* **54** (1995) 97.
6. Mamalis A G, Petrossian G L, and Manolakos D E, *J Mater Process Technol* **96** (1999) 117.
7. Mamalis A G, Petrossian G L, and Manolakos D E, *J Mater Process Technol* **98** (2001) 335.
8. Joseph Davidson M, *Simulation and Analysis of Deformation Characteristics of Sintered Aluminium Preforms During Cold Upset Forming*, M.E Thesis, Anna University, India (2004).
9. Selvakumar N, Radha P, Narayanasamy R, and Joseph Davidson M, *Model Simul Mater Sci Eng* **12** (2004) 611.
10. Gunaraj V, and Murugan N, *J Mater Process Technol* **88** (1999) 266.
11. Montgomery C, *Design and Analysis of Experiments*, 4th edn. Wiley, New York (1997).
12. Jae-Seob K, *Int J Mach Tool Manuf* **45** (2005) 327.
13. Noordin M Y, Venkatesh V C, Sharif S, Elting S, and Abdullah A, *J Mater Process Technol* **145** (2004) 46.
14. Chandrasekhar P, and Singh S, *J Mater Process Technol* **211** (2011) 1285.
15. Ahasan M, and Davidson M J, *Mater Manuf Process* **30** (2015) 1.
16. Rao T B, and Ponugoti G R, *Trans Indian Inst Metals* **74** (2020) 159.
17. Ponugoti G R, Vundavilli P R, Gopala Krishna A, *Adv Manuf Tech* **1**(2019) 485.
18. Zhang X Q, Peng Y H, and Ruan X Y, *J Mater Process Technol* **105** (2000) 253.